

# Multi-frequency study of the BL Lac object PKS 2233–148

A.B. Pushkarev<sup>1,2</sup>, M.S. Butuzova<sup>1</sup>, Y.Y. Kovalev<sup>2,3,4</sup>, T. Hovatta<sup>5</sup>

<sup>1</sup>Crimean Astrophysical Observatory, Russia; <sup>2</sup>Astro Space Center of Lebedev Physical Institute, Russia

<sup>3</sup>Moscow Institute of Physics and Technology, Russia; <sup>4</sup>Max-Planck-Institut für Radioastronomie, Germany; <sup>5</sup>Turku University, Finland

arXiv:1808.06138

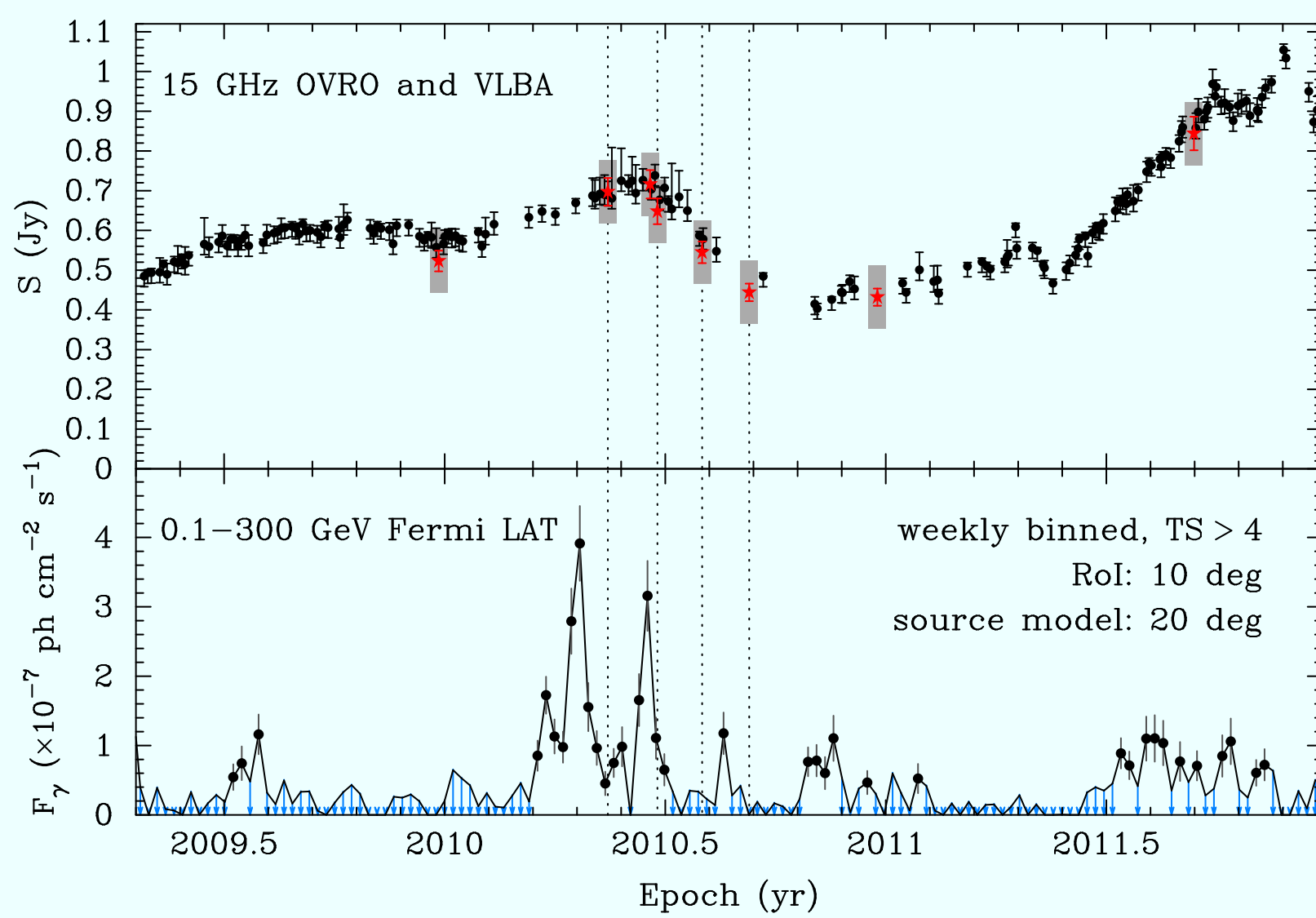


**Fig. 2.** Radio (top) and  $\gamma$ -ray (bottom) light curves. Red stars indicate VLBA total flux density at 15.4 GHz (S2087D + MOJAVE). Upper limits of the  $\gamma$ -ray photon flux are given by blue arrows.

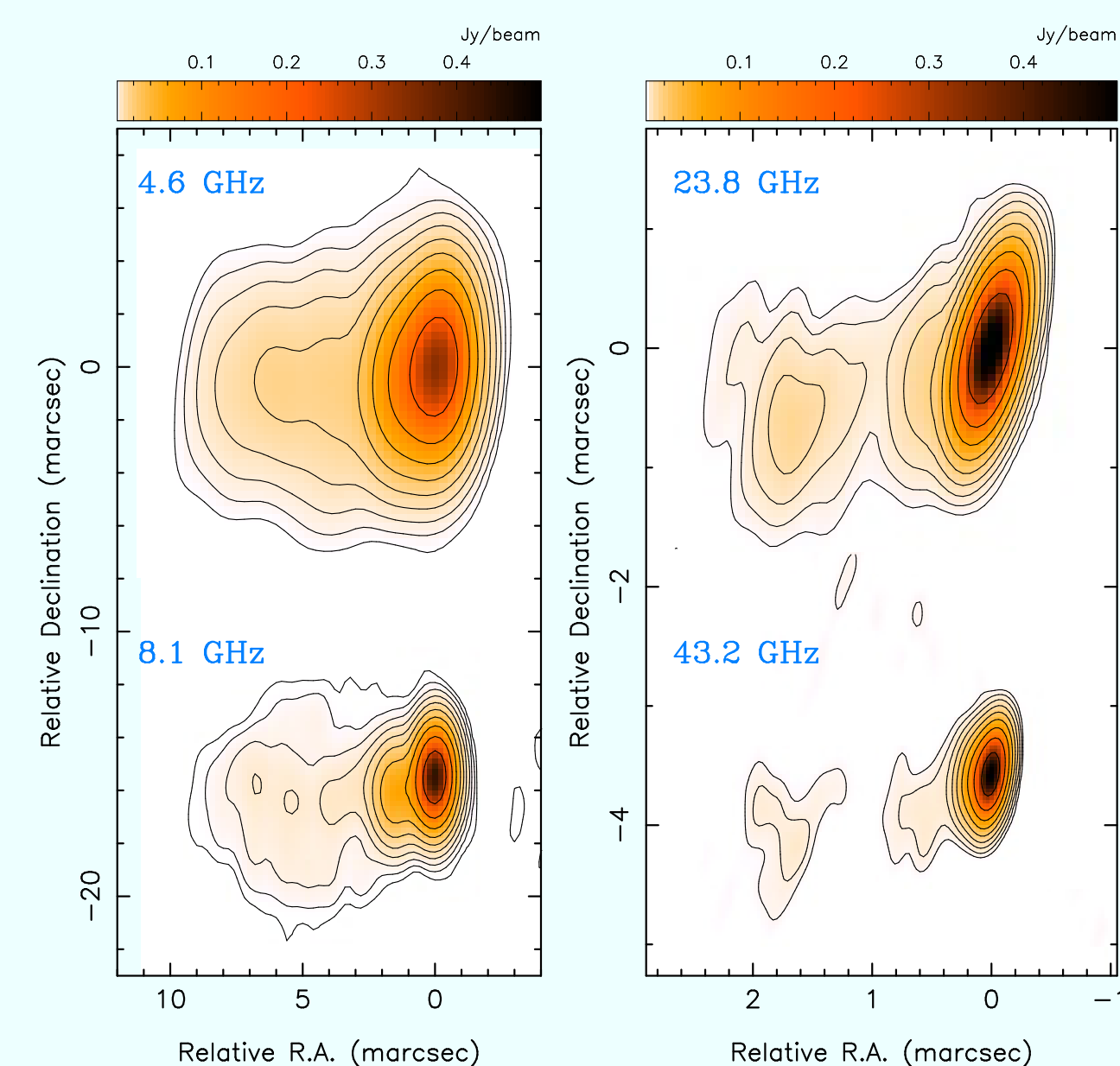


**Fig. 1.** I-maps PKS 2233–148 at epoch 2010-05-15 at 4.6, 8.1, 23.8, and 43.2 GHz. The contours are plotted at increasing powers of  $\sqrt{2}$  starting from 4 rms level.

## Abstract

- We used four-epoch multi-frequency (4–43 GHz) VLBA observations triggered by a flare in  $\gamma$ -rays registered by the *Fermi*-LAT on April 23, 2010. We also used 15 GHz data from the OVRO 40-m telescope and MOJAVE VLBA monitoring programs, and the *Fermi*-LAT data.
- Jet shape of the source is conical setting a lower limit of  $\sim 0.1$  on its unknown redshift. Nuclear opacity is dominated by synchrotron self-absorption, with a wavelength-dependent core shift  $r_{\text{core}}[\text{mas}] \approx 0.1\lambda_{[\text{cm}]}$  mas co-aligned with the innermost jet direction.
- The turnover frequency of the synchrotron spectrum of the VLBI core shifts towards lower frequencies as the flare propagates down the jet, and the speed of this propagation is about 1 mas/yr corresponding to an apparent speed  $\beta_{\text{app}} > 34c$  for  $z > 0.5$ .
- We found indications that the  $\gamma$ -ray production zone in the source is located at large distances, 10–20 pc, from a central engine, and can be associated with the stationary jet features.

## Core shifts and jet shape

Shortly after a flare in  $\gamma$ -rays on April 23, 2010 registered by the *Fermi*-LAT (**Fig. 1**), a series of four VLBA observing sessions was triggered. Each of the session was carried out at 4.6, 5.0, 8.1, 8.4, 15.3, 23.8, and 43.2 GHz. The source shows a short jet to the East (**Fig. 2**).

We measured frequency-dependent shifts of the apparent position of the VLBI core by (i) applying a 2D cross-correlation technique to align the images at different frequencies and (ii) using results of structure model fitting. The core shifts follow a  $\nu^{-1/k_r}$  dependence with  $k_r \approx 1$  suggesting that the flare disturbs only a limited portion of the jet, deviating  $k_r$  in a frequency range significantly narrower than that of our VLBA observations. In **Fig. 3** we show the core shifts as a function of difference of observing wavelengths,  $r_{\text{core}} = a(\lambda_2 - \lambda_1)$ , where  $a \approx 0.1$  mas/cm.

To study a jet shape we fitted a dependence  $d \sim r^b$ , where  $d$  is the jet component size or its resolution limit (Kovalev et al. 2005),  $r$  is the distance to the true jet origin calculated by adding  $r_{\text{core}}(t) = a(t)\lambda$  ( $\lambda_1 = 0$ ). The jet manifests a conical streamline (**Fig. 4**), suggesting that its redshift  $> 0.1$ . Otherwise, we would detect the jet shape transition from parabolic to conical revealed for nearby AGN jets (e.g., Asada & Nakamura 2012; Kovalev et al. in prep.).

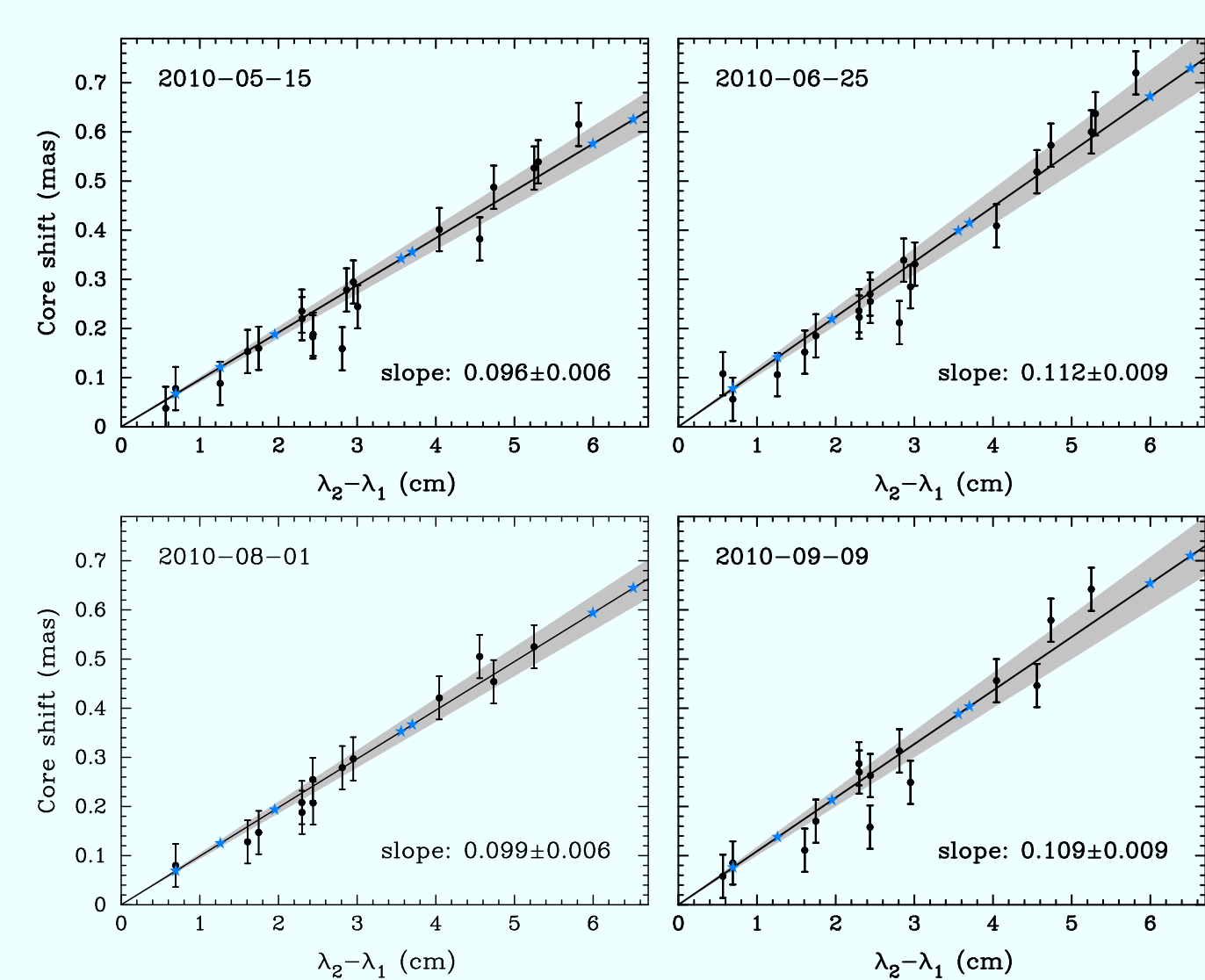


**Fig. 3.** Core shifts as a function of difference of observing wavelengths. Shaded areas show  $1\sigma$  confidence regions of the fit. Stars denote the expected core shifts from the true jet origin ( $\lambda_1 = 0$ ) at wavelengths of our observations, 0.7, 1.3, 2.0, 3.6, 3.7, 6.0, 6.5 cm.

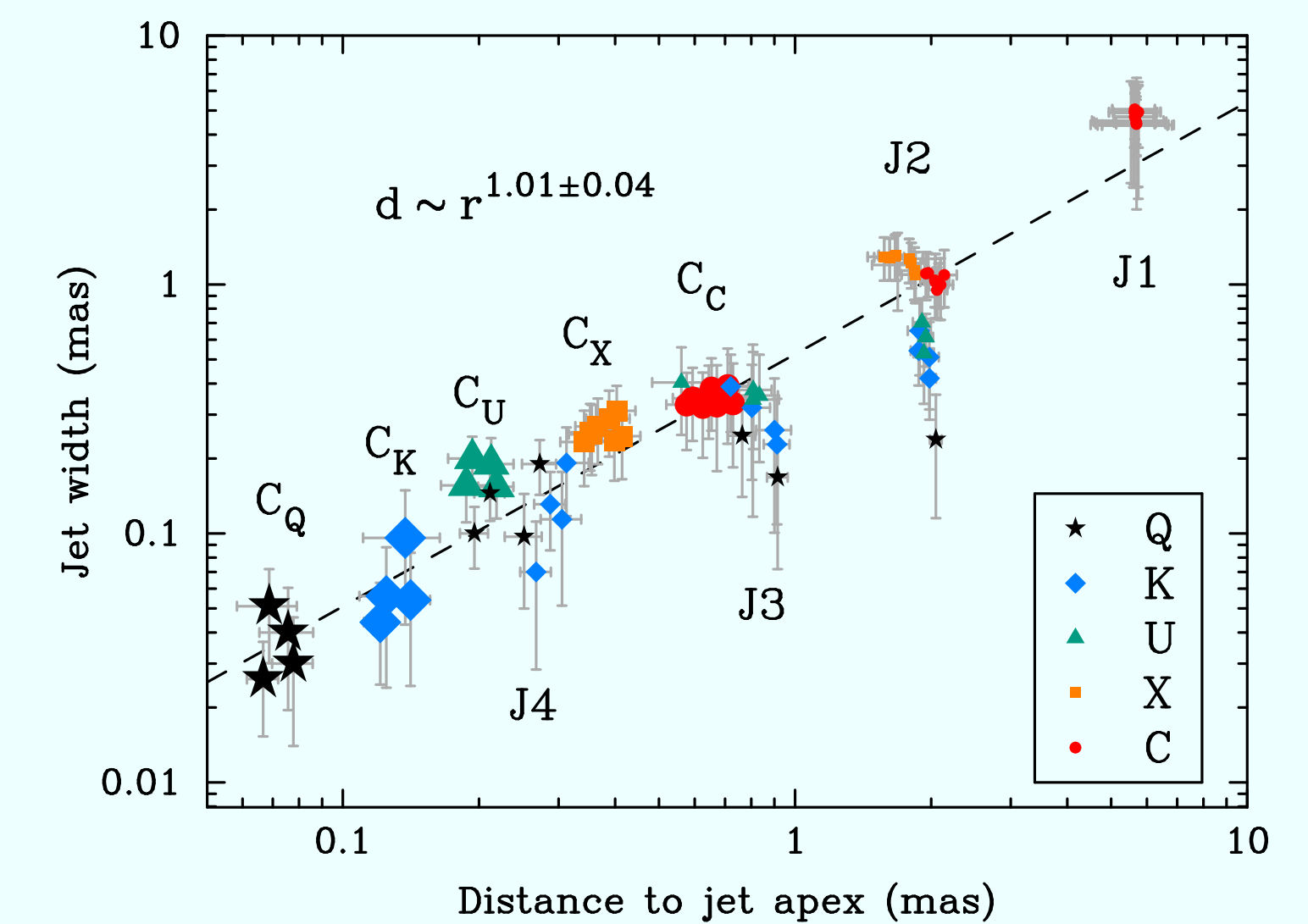


**Fig. 4.** Jet width versus distance to the jet vertex for core and jet components from structure model fits at 7 frequencies of 4 epochs. Cores are marked by larger symbols. The jet shape as probed by our multi-frequency VLBA observations is conical.

## Synchrotron spectrum evolution and source kinematics

Spectral index distribution map (**Fig. 5**) shows optically thin jet with  $\alpha_{\text{jet}} \approx -1$  and partially opaque core with  $\alpha_{\text{core}} \approx 0.3$ . We fitted the VLBI core data with the standard spectrum of a homogeneous incoherent synchrotron source of relativistic plasma with a power-law energy distribution (**Fig. 6**). Best fit parameters are the optically thin spectral index, the peak flux density  $S_m$  and the corresponding self-absorption turnover frequency  $\nu_m$ . The latter decreases from  $16.8 \pm 5.3$  GHz on May 15, 2010 to  $6.4 \pm 1.1$  GHz on September 9, 2010 following  $\nu_m \propto t^{-1}$  dependence and reflecting a flare propagation downstream. Due to synchrotron opacity in the nuclear region, the flare developing along the jet becomes detectable at progressively larger distances from the true jet origin corresponding to the VLBI core locations  $r_{\text{core}} = r_{\text{flare}} = a(t)\lambda_m(t)$  at longer wavelengths.

In **Fig. 7** we show  $r_{\text{flare}}(\lambda_m)$  as a function of time. The slope of the weighted linear fit is  $\mu = 1.14 \pm 0.07$  mas yr<sup>-1</sup> corresponding to apparent speed  $\beta_{\text{app}} > 34 \pm 2c$ , if we assume  $z > 0.5$  reported by Sbarufatti et al. 2006. It is much faster than a typical apparent speed  $\approx 4c$  derived from kinematics analysis for a sample of 42 BL Lacs (Lister et al. 2016).

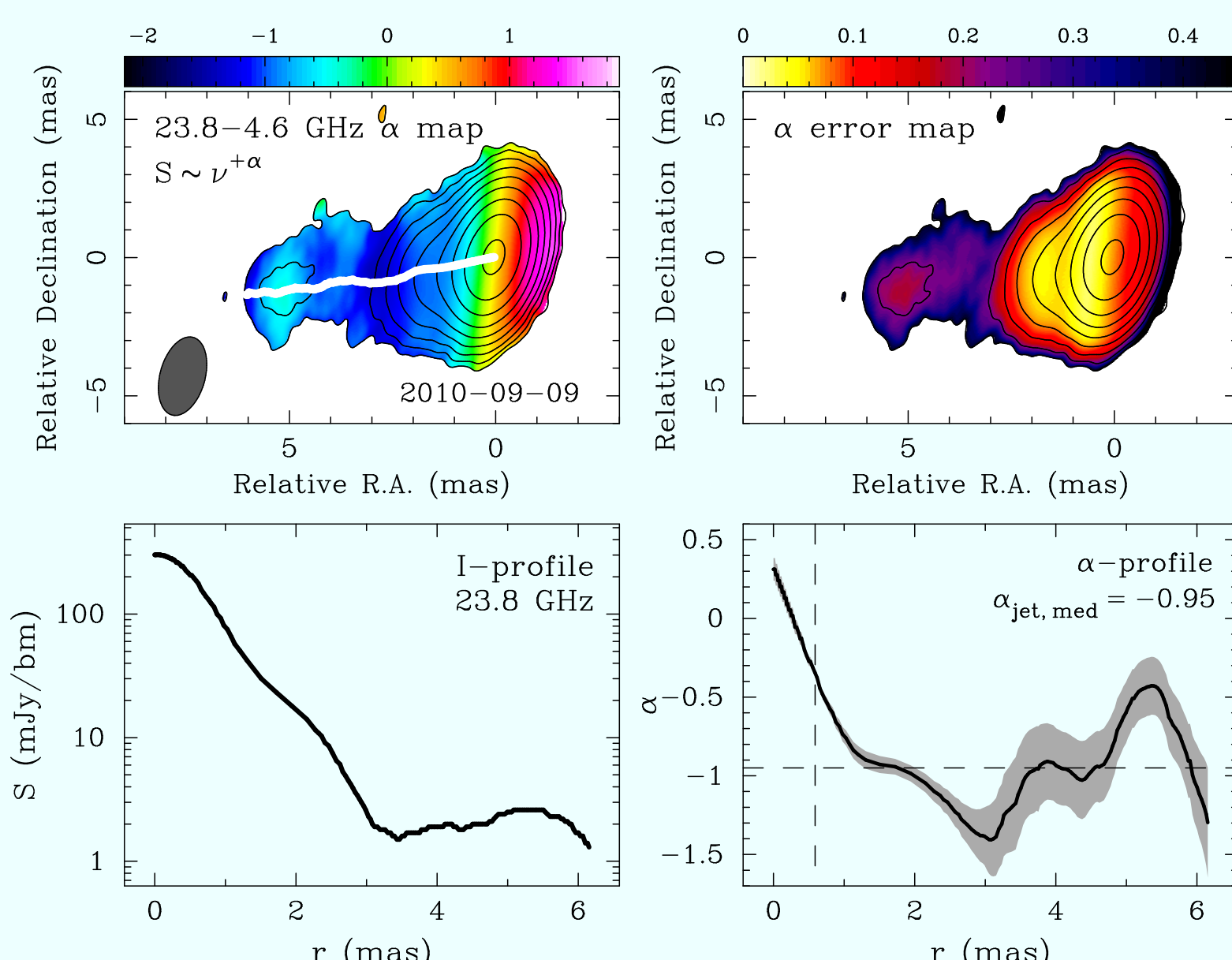


**Fig. 5.** Distribution of spectral index (top left) at the epoch 2010-09-09 between 4.6 and 23.8 GHz shown in color, with the 23.8 GHz I contours overlaid. White curve denotes the total intensity ridgeline, along which I (bottom left) and  $\alpha$  (bottom right) slices are taken.

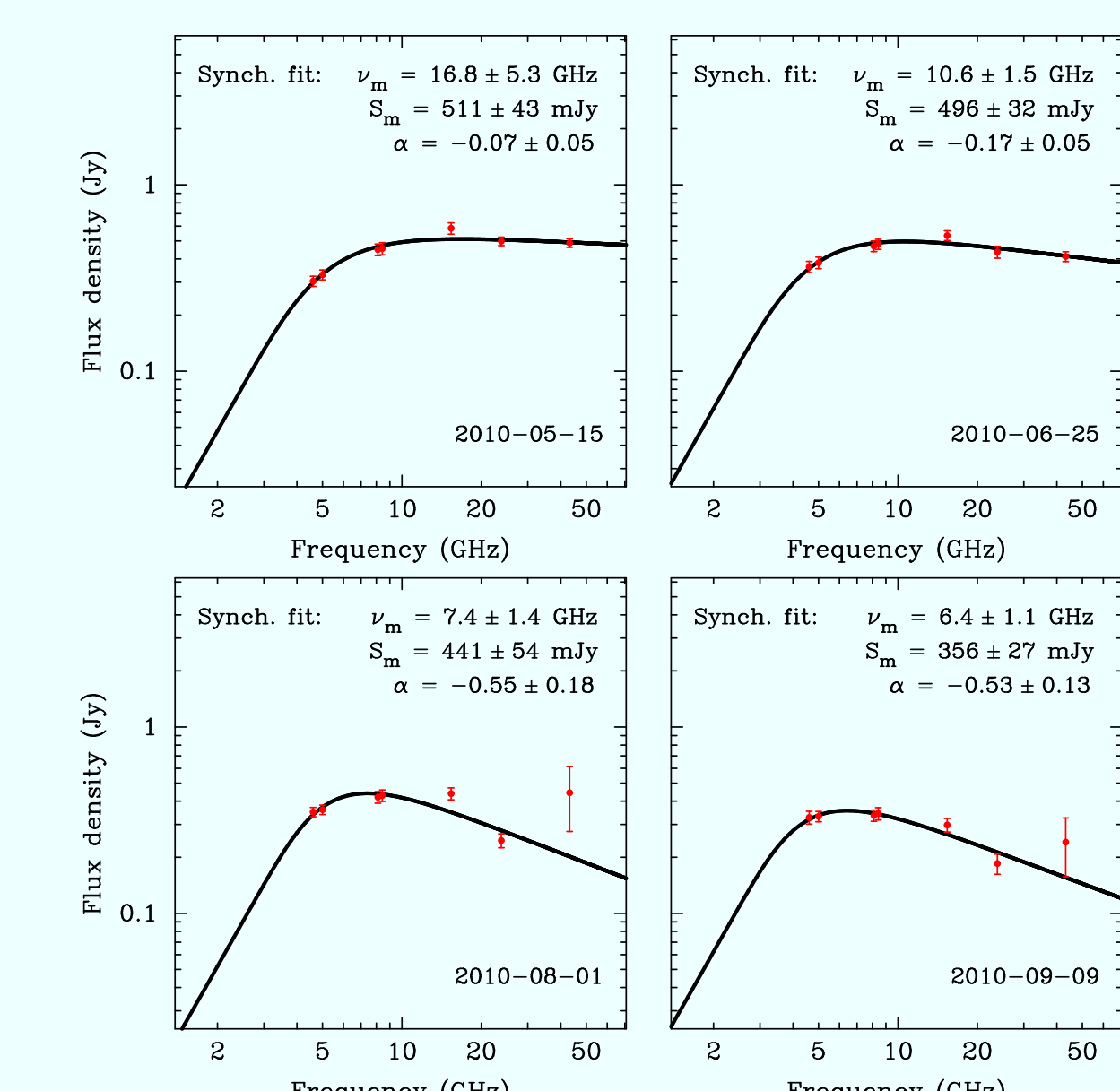


**Fig. 6.** Spectral fits to the core data. Solid lines represent the spectra derived from the homogeneous synchrotron source model. Best fit parameters of models are shown on each plot.

## Gamma-ray emission zone and HE-mechanisms

To estimate the location of the  $\gamma$ -ray emission zone in PKS 2233–148 we extrapolated the  $r_{\text{flare}}$  dependence (**Fig. 7**) back to the epoch of the  $\gamma$ -ray flare, 2010.31 (**Fig. 1**). This yields an angular separation of  $0.12 \pm 0.03$  mas from the true jet base, which corresponds to the VLBI core position at 24 GHz (**Fig. 4**). In linear scale it is  $> 0.7 \pm 0.2$  pc in projection ( $z > 0.5$ ) and  $> 8 \pm 2$  pc de-projected assuming a jet viewing angle of  $5^\circ$ . Considering the second peak of the  $\gamma$ -ray data at epoch 2010.46, we inferred distance of  $\sim 0.3$  mas from the jet apex. It corresponds to the innermost jet feature J4 detected at 24 and 43 GHz setting an absolute distance of about 20 pc for another possible location of the  $\gamma$ -ray emission site.

At these large distances the dusty torus is no longer effective as a source of infrared photons. Instead, synchrotron self-Compton is likely a dominant high-energy emission mechanism. We also revealed a direct observational evidence for a boundary layer around the jet (**Fig. 8**) suggesting that the slow sheath might be an additional photon field for external Compton scattering acting in the source (e.g. Marscher et al. 2010; Aleksić et al. 2014).

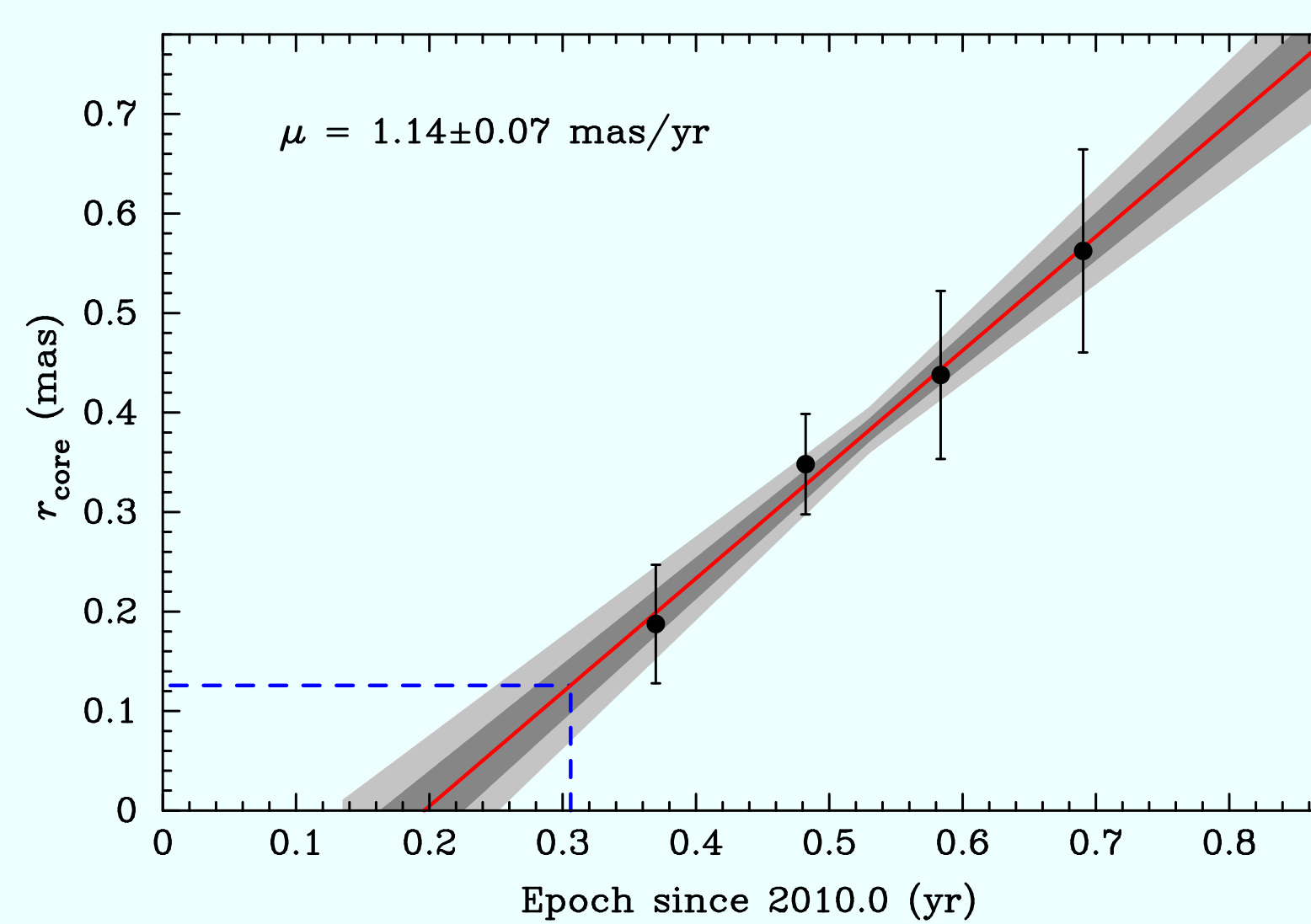


**Fig. 7.** Evolution of the turnover frequency (Fig. 6) of the VLBI core as a function of time. Dot-dashed lines indicate the epoch 2010.31 of the  $\gamma$ -ray flare and the corresponding distance 0.12 mas of the  $\gamma$ -ray emission zone from the central engine.

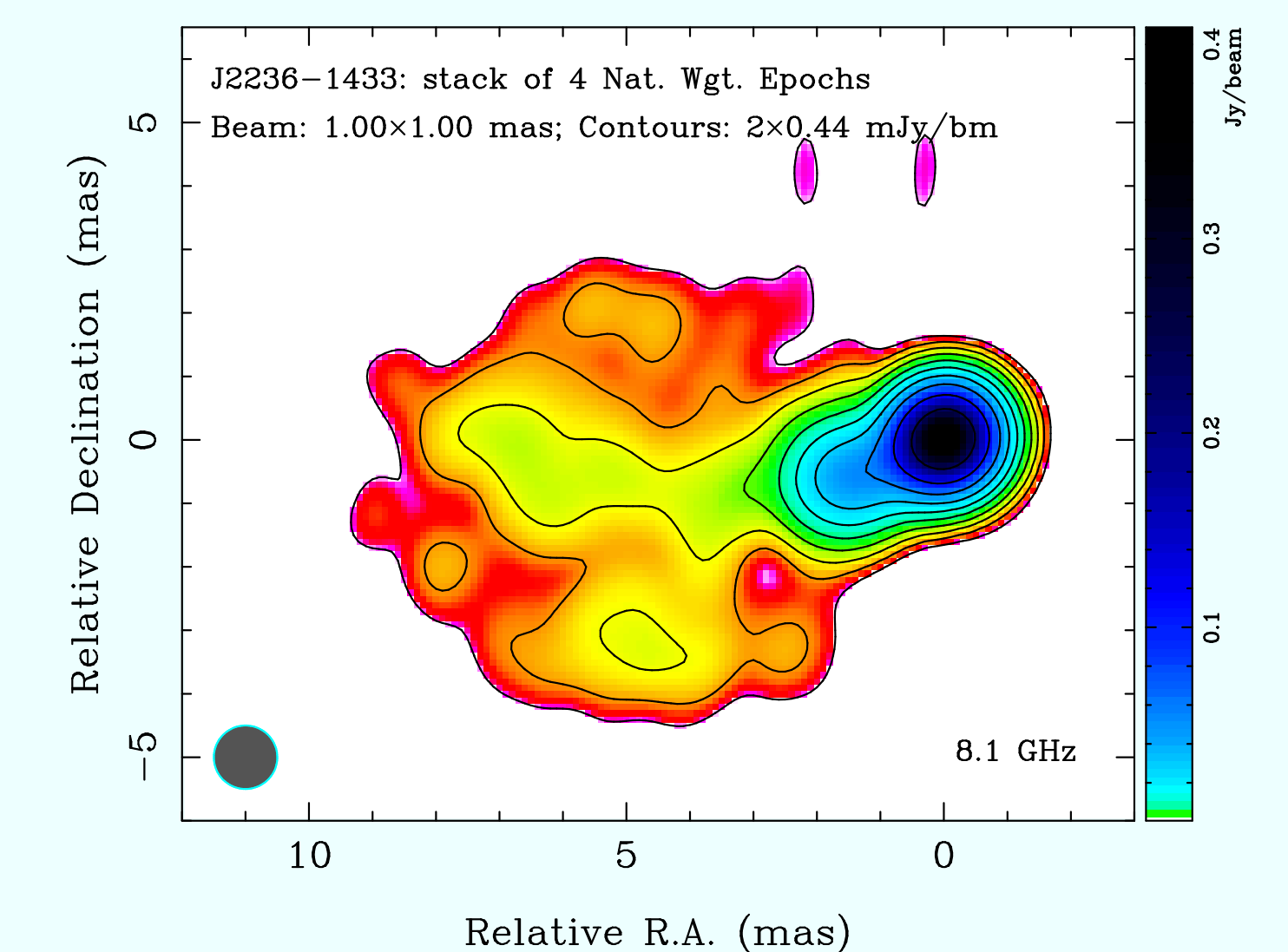


**Fig. 8.** Total intensity map of PKS 2233–148 at 8.1 GHz stacked over the four epochs and convolved with a 1 mas circular beam. Emission at the jet edges (reddish and yellowish colors) indicate a presence of a boundary layer around the jet.

## References

- Aleksić J., Ansoldi S., Antonelli L. A., Antoranz P., Babic A., et al., 2014, *A&A*, 569, A46  
 Asada K., Nakamura M., 2012, *ApJ*, 745, L28  
 Deller A. T., Bricken W. F., Phillips C. J., et al., 2011, *PASP*, 123, 275  
 Kovalev Y. Y., Kellermann K. I., Lister M. L., Homan D. C., Vermeulen R. C., Cohen M. C., et al., 2005, *AJ*, 130, 2473  
 Lister M. L., Aller M. F., Aller H. D., Kellermann K. I., Kovalev Y. Y., Pushkarev A. B., Richards J. L., et al., 2016, *AJ*, 152, 12  
 Lister M. L., Aller M. F., Aller H. D., Hodge M. A., Homan D. C., Kovalev Y. Y., Pushkarev A. B., Savolainen T., 2018, *ApJS*, 234, 12  
 Marscher A. P., Jorstad S. G., Larionov V. M., Aller M. F., Aller H. D., et al., 2010, *ApJ*, 710, L126  
 Sbarufatti B., Treves A., Falomo R., Heidt J., Kotilainen J., Scarpa R., 2006, *AJ*, 132, 1  
 Richards J. L., Max-Moerbeck, W., Pavlidou, V., et al., 2011, *ApJS*, 194, 29

## Acknowledgements

The VLBA data processing and core shift analysis were supported by the Russian Science Foundation grant 16-12-10481. The radio/ $\gamma$ -ray joint analysis was supported by the Academy of Finland projects 296010 and 318431. T.H. acknowledges support from the Turku Collegium of Science and Medicine. This research has made use of data from the MOJAVE data base, which is maintained by the MOJAVE team (Lister et al. 2018). The MOJAVE project was supported by NASA-*Fermi* GI grants NNX08AV67G, NNX12A087G, and NNX15AU76G. This work made use of the Swinburne University of Technology software correlator (Deller et al. 2011), developed as part of the Australian Major National Research Facilities Programme and operated under licence. This research has made use of data from the OVRO 40-m monitoring program (Richards et al. 2011) which is supported in part by NASA grants NNX08AW31G, NNX11A043G, and NNX14AQ89G and NSF grants AST-0808050 and AST-1109911. The National Radio Astronomy Observatory is a facility of the National Science Foundation operated under cooperative agreement by Associated Universities, Inc.